Combining systems and synthetic biology for *in vivo* enzymology

Sara Castaño-Cerezo[1], Alexandre Chamas[2,†], Hanna Kulyk[1,3], Christian Treitz[4], Floriant Bellvert[1,3], Andreas Tholey[4], Virginie Galéote[2], Carole Camarasa[2], Stéphanie Heux[1], Luis F. Garcia-Alles[1], Pierre Millard[1,3,*] and Gilles Truan[1,*]

[1]TBI, Université de Toulouse, CNRS, INRAE, INSA, Toulouse, France

[2]SPO, Université Montpellier, INRAE, Institut Agro Montpellier, Montpellier, France

[3]MetaboHUB-MetaToul, National Infrastructure of Metabolomics and Fluxomics, Toulouse, France

[4]Systematic Proteome Research and Bioanalytics, Institute for Experimental Medicine, Christian-Albrechts-Universität zu Kiel, Kiel, Germany

[†]current address: Department of Microbial Pathogenicity Mechanisms, Leibniz Institute for Natural Product Research and Infection Biology (HKI), Jena, Germany; Cluster of Excellence Balance of the Microverse, Friedrich Schiller University Jena, Jena, Germany

*to whom correspondence should be addressed: truan@insa-toulouse.fr ; millard@insa-toulouse.fr

Abstract

Enzymatic parameters are classically determined *in vitro*, under conditions that are far from those encountered in cells, casting doubt on their physiological relevance. We developed a generic approach combining tools from synthetic and systems biology to measure enzymatic parameters *in vivo*. In the context of a synthetic carotenoid pathway in *Saccharomyces cerevisiae*, we focused on a phytoene synthase and three phytoene desaturases, which are difficult to study *in vitro*. We designed, built, and analyzed a collection of yeast strains mimicking substantial variations in substrate concentration by strategically manipulating the expression of geranyl-geranyl pyrophosphate (GGPP) synthase. We successfully determined *in vivo* Michaelis-Menten parameters (K_M, V_{max} and k_{cat}) for GGPP-converting phytoene synthase from absolute metabolomics, fluxomics and proteomics data, highlighting differences between *in vivo* and *in vitro* parameters. Leveraging the versatility of the same set of strains, we then extracted enzymatic parameters for two of the three phytoene desaturases. Our approach demonstrates the feasibility of assessing enzymatic parameters directly *in vivo*, providing a novel perspective on the kinetic characteristics of enzymes in real cellular conditions.

Introduction

Enzymes catalyze most of the chemical reactions in living systems. A comprehensive interpretation of enzymatic parameters is therefore of paramount importance to grasp the complexity of cellular metabolism. The vast amount of data collected for thousands of enzymes has contributed to significant progress in our understanding of the remarkable chemical capabilities of biocatalysts and of their roles in cellular reactions.

Enzymatic reactions are traditionally analyzed *in vitro*, under dilute conditions, using pure or semi-pure protein samples in buffer solution. In contrast, the cellular medium is most accurately viewed as a heterogeneous, dense, crowded gel, containing various types of macromolecules and cellular lipidic organelles, with potential partitioning effects and variations in substrate and/or product diffusion coefficients (1). The parameters determined in classical enzymology experiments may therefore not be representative of *in vivo* reaction rates and equilibrium constants (2, 3). While some progress has been made in implementing and understanding viscosity and crowding effects in *in vitro* enzymatic assays, these conditions do not mimic the intrinsic complexity of the cellular environment (2).

In vivo enzymology seems to be the obvious approach to measure enzymatic parameters inside cells. Early attempts were made using the enzyme photolyase, for which both *in vitro* and *in vivo* parameters were determined (4, 5). Meanwhile, the *in vivo* V_{max} values of ten central carbon metabolism enzymes determined in the early 90s revealed significant differences between *in vivo* and *in vitro* assays for heteromeric protein complexes (6). The past ten years have seen growing interest from systems biology in determining the *in vivo* k_{cat} of native enzymes in model organisms. The *in vivo* apparent k_{cat} of *E. coli* enzymes have been determined independently by two research groups, leveraging advances in absolute protein quantification and high throughput metabolomics (7, 8). These values were obtained by dividing the flux of enzymatic reactions by the absolute abundance of the corresponding enzymes. Both studies found correlations between *in vivo* and *in vitro* data (with correlation coefficients around 0.6), suggesting that this method could serve as an alternative to *in vitro* assays. While this systems biology approach has provided valuable information, it cannot be employed to determine apparent K_Ms *in vivo*. Zotter et al. measured the activity and affinity of TEM1-β lactamase in mammalian cells *in vivo* with confocal microscopy, using a fluorescently tagged enzyme and a fluorescent substrate and product (9). They observed that the catalytic efficiency (k_{cat}/K_M) of this enzyme differs *in vitro* and *in vivo* due to substrate attenuation, indicating that *in vitro* data are not always indicative of *in vivo* function. Zotter et al. is probably the most comprehensive *in vivo* enzymology study to date, but this approach cannot be generalized because of a lack of universally appropriate fluorescent substrates/products for all enzymes. In a recent investigation of the *in vivo* kinetic parameters of thymidylate kinase (TmK), an interesting finding was the difference in TmK's activity pattern when the substrate (thymidine monophosphate, TMP) was supplied in the media versus provided by internal metabolism, with Michaelis-Menten kinetics in the former and Hill-like kinetics in the latter. The authors hypothesized that the limited diffusion of TMP might be due to its confinement in a putative metabolon in *E. coli* (10).

In vivo enzymology is a particularly attractive prospect for membrane and multimeric proteins (6), which are tedious to purify and for which activity assays are difficult to optimize, mostly because artificial membranes are required (11–15). In the industrially important carotenoid pathway for example, despite the expression of numerous carotene biosynthesis enzymes, our understanding of their enzymatic behavior remains limited because many are membrane-associated proteins. While

kinetic parameters for some phytoene synthases, sourced from plants or bacteria, have been established *in vitro*, many enzymatic assays require the co-expression of geranylgeranyl pyrophosphate (GGPP) synthase to attain activity, possibly because of the amphiphilic nature of the substrate or the requirement of membranes (12, 15). Another example of the difficulty of *in vitro* assays is phytoene desaturase, for which discernible enzyme activity has only been achieved in engineered environments (e.g. liposomes) with cell-purified substrate (14, 16–18).

This study combines synthetic and systems biology tools to develop an original *in vivo* enzymology approach. Synthetic biology offers a remarkable set of genetic engineering tools to precisely modulate the activity of enzymes in synthetic pathways, enabling *in vivo* control of substrate concentrations for the studied enzymatic reactions. In turn, systems biology can provide quantitative data on these reactions (fluxes and enzyme, substrate and product concentrations) and computational tools to model their behavior. We applied this approach to investigate a synthetic carotenoid production pathway in *Saccharomyces cerevisiae*, with industrial applications ranging from foods to pharmaceuticals.

Results

General principle of the proposed *in vivo* enzymology method

Enzymes are usually characterized in terms of their affinity (K_M) and activity (maximal reaction rate V_{max} and turnover number k_{cat}) (Fig 1). These parameters are typically determined *in vitro* by varying the substrate concentration across a relatively broad range (about two orders of magnitude) and measuring the reaction rate for each substrate concentration (19). Different mathematical formulas, such as the Michaelis-Menten equation, have been derived to estimate enzymatic parameters from these data. We propose a novel approach wherein the substrate concentration is varied directly within cells (Fig 1), by modulating the concentration of the enzyme producing the substrate of the studied reaction. Levels of the substrate-producing enzyme are varied using different combinations of promoter strengths and gene copy numbers, and translate into a wide range of substrate concentrations (2-3 orders of magnitude, as detailed in the following sections). In our experimental setup, each substrate concentration is achieved using a specifically engineered yeast strain. In each of these strains, the gene encoding the enzyme of interest is expressed at a given level, mirroring the conditions of *in vitro* experiments. Engineered strains are then grown under steady-state conditions (i.e., exponential growth), where reaction fluxes and metabolite concentrations remain constant (20). This stability allows for the accurate measurement of product formation fluxes (equivalent to reaction rates), intracellular substrate concentrations, and enzyme concentrations. The data obtained can then be combined to calculate apparent *in vivo* kinetics parameters, denoted $K_{1/2}^{\mathrm{cell}}$, $\mathrm{V}_{\mathrm{max}}^{\mathrm{cell}}$ and $k_{\mathrm{cat}}^{\mathrm{cell}}$ in analogy with the classical K_M, V_{max} and k_{cat} parameters (Fig 1).

Construction of yeast strains to investigate a synthetic carotenoid production pathway

We evaluated our strategy by investigating a synthetic carotenoid pathway in yeast (*S. cerevisiae*), an industrially important chassis in biotechnology, which includes two membrane-interacting enzymes that are challenging to investigate *in vitro* (12, 16, 17, 21): phytoene synthase (CrtB) and phytoene desaturase (CrtI). Phytoene synthase, the first enzyme in the carotenoid pathway and considered the

119 bottleneck of carotenoid biosynthesis in plants (21), condenses two molecules of geranylgeranyl
120 pyrophosphate (GGPP) head-to-head to form phytoene. Phytoene synthases have proved difficult to
121 express in soluble and active forms in microorganisms (12, 15, 21). *In vitro* rates and affinity
122 constants have been determined for both plant and bacterial phytoene synthases but these
123 parameters may have been altered by the conditions of the *in vitro* assays—adding detergents for
124 the bacterial enzyme and co-expressing a GGPP synthase or using semi-crude extracts for the plant
125 enzyme (12, 15, 21–24). Following this enzymatic step, three insaturations are introduced in
126 phytoene to produce lycopene. In non-photosynthetic bacteria and fungi, three reaction steps are
127 catalyzed by a single enzyme (CrtI in bacteria and CarB in fungi) (25), whereas in plants and
128 cyanobacteria, four different enzymes are involved in the conversion of phytoene to lycopene (26).
129 Given that these desaturation steps are a major bottleneck in microbial carotenoid biosynthesis,
130 determining *in vivo* enzymatic constants is an industrially relevant challenge (10, 22, 23).

131 To analyze these enzymes, we assembled a set of strains covering a broad range of substrate
132 concentrations (Fig 2 and Table EV1). To create the collection of strains with different intracellular
133 levels of GGPP, the substrate of phytoene synthase, we first increased GGPP production by modifying
134 the native terpene pathway: strong constitutional expression of *ERG20* and of the truncated form of
135 *HMG1* and deletion of the main phosphatase gene involved in GGPP and FPP pyrophosphate group
136 removal (*DPP1*), yielding the strain yENZ15 (29, 30). Three different integration cassettes containing
137 different microbial GGPP synthases (CrtE) expressed under different constitutive promoters were
138 integrated into the yENZ15 genome, yielding a series of strains designed to produce a wide range of
139 GGPP concentrations (Fig 2).

140 We then verified that the intracellular GGPP concentration was indeed modulated *in vivo*, as done
141 previously (24, 32–34). GGPP concentration varied by a factor of 38 in these strains (Fig 3B), and the
142 strains all had similar growth rates (0.40±0.03 h^{-1}) (Fig 3B) indicating that there was no change in cell
143 physiology. As detailed below, we used this set of strains as a base to study a phytoene synthase
144 (https://www.uniprot.org/uniprotkb/P21683/entry, EC 2.5.1.32) and three different lycopene-
145 forming phytoene desaturases (EC 1.3.99.31).

146

147 ## *In vivo* enzymatic parameters of phytoene synthase from *Pantoea ananas*

148 We used the set of strains with different intracellular levels of GGPP (Fig 3) to study phytoene
149 synthase from *Pantoea ananas* (PaCrtB) (Fig 4A). In a classical enzymatic reaction setup, enzyme
150 concentration must be carefully controlled to establish an informative set of reaction rate vs
151 substrate concentration data points. To evaluate the impact of enzyme concentration on the
152 collected kinetic profiles, we developed a kinetic model and performed simulations for three
153 different enzyme concentrations (low, medium and high) under a broad range of substrate-producing
154 flux. The relationships between the steady-state substrate concentration and the flux are shown in
155 Fig 4B. Simulation results suggest that excessively high enzyme concentrations would hinder
156 substrate saturation, rendering parameter estimation impossible. In contrast, an extremely low
157 enzyme concentration would lead to a low production flux, making precise measurements difficult
158 and reducing the chance of obtaining accurate enzyme parameters. Therefore, we decided to
159 perform our saturation experiments using three enzyme concentrations by expressing *P. ananas crtB*
160 under the control of three different constitutive promoters (low expression: TEF1mut2p, medium
161 expression: PGI1p and high expression: PDC1p).

162 Consistent with simulation results (Fig 4B), the GGPP concentration progressively decreased as
163 PaCrtB activity increased (Fig 4C). Therefore, the GGPP concentration was very low at high PaCrtB
164 level (PDC1p), and enzyme saturation was not reached. In contrast, the phytoene flux increased as
165 PaCrtB expression increased. The phytoene concentration was too low for accurate quantification of
166 the phytoene flux at low levels of PaCrtB (TEF1mut2p). However, accurate measurements of GGPP
167 concentration and phytoene flux could be made at medium PaCrtB levels (PGIp). Based on these
168 results, we used strains with medium PaCrtB levels for further investigations. A 167-fold variation in
169 GGPP concentration (from 0.12 to 20.78 µM) was observed in these strains. Partial saturation was
170 achieved, leading to a nonlinear relationship between the phytoene flux and the GGPP
171 concentration, as observed in classical *in vitro* experiments. We assumed and verified, by western
172 blot and mass spectrometry-based proteomics, that PaCrtB levels were identical in all strains (Fig EV1
173 and Table EV2), indicating that PaCrtB activity ($\mathrm{V}_{\mathrm{max}}^{\mathrm{cell}}$) was also similar in all strains. Precise estimates
174 of $\mathrm{V}_{\mathrm{max}}^{\mathrm{cell}}$ (849±71 µM/h, rsd = 13 %) and $K_{1/2}^{\mathrm{cell}}$ (19±3 µM, rsd = 14 %) were obtained by fitting these
175 data using an irreversible Michaelis-Menten model (consistent with previous reports (21) and with
176 the very negative ΔG^0 value of this reaction) (Table EV3). As expected from the simulations,
177 parameters could not be determined precisely from the two other datasets (Table EV3). The affinity
178 of PaCrtB for GGPP estimated from our *in vivo* data is higher than measured *in vitro* (K_M = 41 µM)
179 (21), highlighting the necessity of measuring enzyme parameters directly within the intracellular
180 environment. Meanwhile, the $k_{\mathrm{cat}}^{\mathrm{cell}}$ of 6±1 s^{-1}, obtained from absolute quantitative proteomics
181 measurements of the enzyme concentration (42 nM) in strains expressing PaCrtB under the control
182 of PGI1p, is comparable to the one obtained *in vitro* for CrtB in *Pantoea agglomerans* (14 s^{-1}, Table
183 EV4) (15).

184 The theoretical maximum phytoene production flux in these strains is therefore 849±71 µM/h. The
185 bottleneck for carotenoid biosynthesis in plants is phytoene synthase, whose activity is regulated by
186 a combination of transcriptional, post-transcriptional, and post-translational mechanisms to adjust
187 carotenoid production (35). In our synthetic system however, our results suggest that GGPP
188 biosynthesis is the limiting step since five copies of the GGPP synthase gene are required to achieve
189 just 51 % of the maximum phytoene production flux, due to the lack of phytoene synthase
190 saturation.

191

192 **Straightforward extension to analyze downstream enzymes of the carotenoid pathway:**
193 **phytoene desaturases**

194 The most time-consuming tasks in the proposed *in vivo* enzymology protocol are the molecular
195 cloning and strain engineering steps required to generate strains with different substrate
196 concentrations. However, the strains used to investigate a given enzyme can be recycled to
197 investigate downstream steps in the same metabolic pathway, significantly streamlining
198 experiments, which become a simple plug-and-measure process (Fig 5A). Integration of *crtB*,
199 controlled by the high-expression promoter PDC1 into our initial set of strains, produced strains with
200 a 430-fold variation in phytoene concentration (from 4 to 1641 µM). These strains thus form an ideal
201 framework to investigate the *in vivo* kinetics of the next metabolic step with various phytoene
202 desaturases.

203 To demonstrate this point, we chose three widely used microbial lycopene-forming phytoene
204 desaturases (1.3.99.31) (22, 23, 25, 26): *P. ananas* CrtI (P21685, PaCrtI), which, along with *Rubrivivax*

205 *gelatinosus* CrtI, is one of only two lycopene-forming phytoene desaturases with published *in vitro*
206 enzymatic parameters (14, 28); and two fungal CrtIs widely used in carotenoid production, one from
207 *Phaffia rhodozyma*, formely *Xanthophyllomyces dendrorhous* (A0A0P0KMF9, XdCrtI), and the other
208 from *Blakeslea trispora* (Q67GI0, BtCrtI), with no enzymatic data available to date.

209 As for the investigation of phytoene synthase, the expression of the phytoene desaturases was
210 controlled by different promoters: TDH3p for PaCrtI, PGK1p for XdCrtI, and PGI1p for BtCrtI. These
211 promoters were chosen based on the relative lycopene producing abilities of the different CrtIs in *S.*
212 *cerevisiae.* This was especially important for BtCrtI, where high expression in the exponential phase
213 caused cell death due to the formation of lycopene crystals (Fig EV2A). PaCrtI and XdCrtI levels did
214 not vary with the phytoene concentration of the strains, but BtCrtI levels were slightly higher in the
215 strains with the lowest phytoene concentrations (Fig EV3). The higher levels of PaCrtI compared with
216 those of the fungal phytoene desaturases is explained in large part by the use of a TDH3 promoter.
217 However, lycopene fluxes were 10 times lower with PaCrtI than with XdCrtI or BtCrtI (Fig 5). Phytoene
218 levels were high enough to saturate both fungal CrtIs (Fig 5) but not PaCrtI, for which lycopene fluxes
219 remained low for all tested phytoene concentrations.

220 The experimental data from the three enzymes were fitted with an irreversible Michaelis-Menten
221 equation, from which $\mathrm{V}_{\mathrm{max}}^{\mathrm{cell}}$ and $K_{1/2}^{\mathrm{cell}}$ values were successfully obtained for XdCrtI and BtCrtI but not
222 for PaCrtI, for which only lower limits for $\mathrm{V}_{\mathrm{max}}^{\mathrm{cell}}$ (13 μM·h^{-1}) and $K_{1/2}^{\mathrm{cell}}$ (560 μM) could be determined
223 (Table EV3). The $\mathrm{V}_{\mathrm{max}}^{\mathrm{cell}}$ values obtained for BtCrtI (309±22 μM·h^{-1}) was higher than for XdCrtI (168±7
224 μM·h^{-1}), and the $K_{1/2}^{\mathrm{cell}}$ for BtCrtI (41±12 μM) was 9 times smaller than XdCrtI's (380±49 μM). The
225 $k_{\mathrm{cat}}^{\mathrm{cell}}$ obtained by integrating quantitative proteomics measurements in strains expressing XdCrtI
226 under PGK1p was 0.030±0.006 s^{-1} (Table EV3).

227 These results highlight the versatility of our approach to compare the *in vivo* behavior of enzymes
228 from different organisms, using the same set of strains, and provide valuable information to
229 understand and optimize natural and synthetic pathways *in vivo*.

230

231 Discussion

232 Inspired by conventional *in vitro* enzyme assays, we developed an innovative approach to measure
233 enzyme kinetics *in vivo.* We successfully used the proposed method to estimate the *in vivo*
234 equivalents of Michaelis-Menten parameters for a phytoene synthase and two phytoene desaturases
235 in *S. cerevisiae*.

236 These results highlight the reliability and versatility of our *in vivo* enzymology approach, which hinges
237 on solving two methodological challenges: 1) controlling the substrate pool over a broad
238 concentration range, and 2) measuring the total concentrations of substrate, product and enzyme.
239 The first challenge was addressed using synthetic biology tools to modulate the concentration of a
240 substrate-producing enzyme (here GGPP synthase, CrtE). The second challenge was overcome thanks
241 to sensitive, quantitative metabolomics and proteomics techniques that can be generalized to
242 various other enzymatic models. Indeed, the coverage of the metabolome and fluxome by current
243 omics approaches is now high and is continuously increasing, which enables the application of the
244 proposed approach to a broad range of enzymes. In this study, we quantified three basic enzymatic

245 parameters ($K_{1/2}^{\text{cell}}$, $k_{\text{cat}}^{\text{cell}}$ and V_{max}^{cell}). In the absence of absolute quantitative proteomics data, the
246 proposed method still allows for the determination of V_{max}^{cell} and $K_{1/2}^{cell}$ values, providing sufficient
247 information for most enzymology and metabolic engineering studies. Similarly, estimating the
248 absolute $K_{1/2}^{cell}$ values can be achieved using only relative flux values, without requiring absolute
249 concentration of enzymes.

250 We demonstrate that substrate concentrations can be varied *in vivo* over a wide range. Here, the
251 GGPP concentration was varied by a factor 167 and the phytoene concentration by a factor 430,
252 allowing clear enzyme saturation curves to be observed for the two fungal phytoene desaturases
253 (XdCrtI and BtCrtI). However, while the range of substrate concentrations explored was significantly
254 wider than those used in *in vitro* studies of the same enzymes (Table EV4) (16, 21), complete
255 saturation was not achieved for PaCrtB or PaCrtI. It is conceivable that, when these enzymes are
256 bound to natural membranes, their apparent affinity for the substrate could differ from the *in vitro*
257 environment. A second explanation concerns substrate availability. While classical *in vitro* enzyme
258 assays involve homogeneous, highly diluted buffers, the intracellular environment is dense,
259 heterogeneous and compartmentalized. In this first *in vivo* approach, variations in substrate
260 concentrations between compartments were not considered explicitly, though it may have affected
261 the values obtained for the parameters. For example, a higher concentration of phytoene inside lipid
262 droplets compared with the rest of the membrane would reduce phytoene concentrations around
263 CrtI enzymes and would thus limit substrate saturation. Enzyme localization could also affect
264 measurements as conditions (pH, concentration of ions, etc.) vary between compartments. Iwata-
265 Reuyl et al. found for instance that the measured activity of PaCrtB is 2,000 times lower in the
266 absence of detergents (15), and Fournié et Truan observed that different heterologous CrtI
267 expression systems produced different phytoene saturation patterns (36). In the case of the two *P.*
268 *ananas* enzymes, the mechanisms that cause the absence of saturation may be different. For PaCrtI,
269 the observed concentrations of phytoene (substrate) and lycopene (product) are either equivalent to
270 or lower than those obtained with the two fungal CrtI enzymes. This suggests a true difference in the
271 affinity for phytoene between the bacterial and fungal enzymes. For PaCrtB, given that the GGPP
272 concentration in the cell is high (around 20 µM), the lack of complete saturation is more likely due to
273 a heterogeneous distribution of GGPP within the cell, with only a fraction of GGPP being in the
274 vicinity of the enzyme. Dedicated studies will be required to clarify the effects of cell compartments
275 on enzyme efficiency.

276 In addition, other explanations for the difficulty in reaching complete saturation merit attention as
277 they also convey general hypotheses on metabolic systems: i) substrate or product toxicity
278 detrimental to cell growth (e.g. the specific growth rate is nearly 50 % lower for lycopene
279 concentrations above 400 µM, (Fig EV2B), ii) overflow mechanisms that relocate some of the
280 substrate to a different cell compartment or even outside the cell (37, 38), iii) the presence of
281 alternative pathways that divert additional substrate produced above a certain concentration
282 threshold (39, 40), or iv) intrinsic properties of metabolic systems whereby production fluxes tend to
283 decrease when product concentrations increase (41–43). While these mechanisms contribute to
284 global metabolite homeostasis (44–46) and are essential for cell viability, they limit substrate
285 accumulation and thus could prevent complete saturation of the enzyme. Moreover, it is crucial to
286 bear in mind that, similarly to *in vitro* data, enzymatic parameters are only valid under the conditions
287 used to measure them. We therefore argue that enzymatic parameters should not be considered
288 constants since they depend on the microenvironment (pH, ion concentration, temperature,

289 membrane composition, etc.), be that *in vitro* or *in vivo*. Still, as mentioned below, these parameters
290 are useful for pathway engineering and an advantage of our *in vivo* enzymology method is that
291 kinetics parameters are measured under the exact same conditions as the enzyme is expressed.

292 Our approach enables the determination of whether a given enzyme is operating at saturation *in vivo*
293 under different cellular conditions. The tested enzymes displayed various saturation profiles,
294 indicating that they may function under diverse conditions within the cell. Operating at full
295 saturation (far above the $K_{1/2}^{\mathrm{cell}}$, the enzyme works at its maximum rate, being unaffected by changes
296 in substrate concentration or minor environmental variations. This makes the enzymatic reaction
297 highly robust in terms of product formation. Conversely, if an enzyme operates at substrate
298 concentrations much lower than the $K_{1/2}^{\mathrm{cell}}$, any variation in substrate concentration will directly affect
299 the production rate. This could maintain substrate homeostasis, potentially prevent toxic effects due
300 to concentration changes. From a metabolic engineering perspective, achieving the optimal balance
301 between high product formation and metabolic homeostasis is crucial. This balance can be attained
302 by adjusting the levels of both the substrate-forming enzyme and the target enzyme. This process
303 needs to be repeated for each enzyme, potentially under different saturation regimes. In
304 biotechnology, our *in vivo* enzymology approach may thus guide metabolic engineering strategies to
305 ensure that the overall pathway maintains the desired balance between production and cellular
306 homeostasis, thereby ensuring greater stability and robustness of the engineered microbial strains at
307 maximal production flux.

308 The final step in our *in vivo* enzymology method involves fitting experimental data with a
309 mathematical model of enzyme kinetics to obtain the corresponding parameters, the same approach
310 as used *in vitro*. Traditional enzymatic models were derived with *in vitro* measurements and
311 assumptions in mind. For instance, the classical Michaelis-Menten relationship applies only at steady-
312 state, a condition clearly met in our experimental setup where all data were collected during
313 exponential growth (i.e. metabolite concentrations and fluxes remain constant over time). However,
314 other assumptions do not hold *in vivo*, in particular regarding the product concentration, which
315 cannot be zero. Nevertheless, for the enzymes investigated here, where the catalyzed reactions are
316 essentially irreversible, the reverse reaction can be neglected, and the Michaelis-Menten formalism
317 still applies. Another important assumption is that the substrate concentration must be higher than
318 the enzyme concentration. In this study, the *in vivo* substrate/enzyme ratio was between 8 and 1400
319 for PaCrtB and between 2 and 2500 for XdCrtI (Table EV5). Surprisingly, this criterion was not met for
320 CrtB and CrtI in previous *in vitro* assays (19, 37), with substrate/enzyme ratios between 0.05 and 0.18
321 for PaCrtB and between 1 and 2.57 for PaCrtI (Table EV4). In our setup, despite some formal
322 assumptions not being fully satisfied, the data were still satisfactorily fit with a Michaelis-Menten
323 equation. This underscores the applicability of our method, from which informative parameters such
324 as the degree of saturation can be inferred to understand *in vivo* enzyme function and to engineer
325 natural and synthetic pathways for biotechnology. The availability of *in vivo* data about enzyme
326 kinetics may also lead to the derivation of specific laws that account for the specificities of *in vivo*
327 studies (e.g., non-negligible product concentrations).

328 As we advocate for the simplicity of our method, we would like to share some insights on its
329 implementation in future studies. First, to maximize the output of genetic constructs, experimental
330 design should be employed to compare various enzymes that catalyze the same reaction (whether
331 mutants or from different species) or to target multiple enzymes in the same metabolic pathway, in

332 this case phytoene synthase and phytoene desaturase. Second, the number of genetic constructs
333 necessary to reach saturation (ideally 4 to 5) can be minimized by verifying the substrate production
334 range early on. Third, in most cases, testing three enzyme concentrations has been sufficient to
335 obtain a satisfactory saturation curve or at least to precisely estimate the $K_{1/2}^{\text{cell}}$ range. Lastly,
336 improvements can be made using high-throughput methods for the construction of plasmids and
337 strains, for growth experiments and for samples preparation steps. The development of single cell
338 metabolomics and proteomics approaches will also significantly increase the throughput of the strain
339 characterization step in future studies.

340 Sixteen years ago, in their review on enzyme function, Dagmar Ringe and Gregory Petsko wrote:
341 "How do enzymes function in a crowded medium of low water activity, where there may be no such
342 thing as a freely diffusing, isolated protein molecule? *In vivo* enzymology is the logical next step along
343 the road that Phillips, Koshland, and their predecessors and successors have traveled so brilliantly so
344 far" (3). The work presented here, albeit performed in the context of a synthetic metabolic pathway,
345 touches on the difference between kinetic parameters measured *in vitro* and *in vivo* and their
346 interpretation. We notably show how fine-tuning and balancing the expression of the substrate-
347 producing enzyme and the enzyme under study yields datasets from which meaningful and reliable
348 enzymatic parameters ($K_{1/2}^{\text{cell}}$, $k_{\text{cat}}^{\text{cell}}$ and V_{max}^{cell}) can be obtained. By including additional controlled
349 steps, this method could be applied to a wider range of variables, such as inhibition and activation
350 parameters (by modulating the pool of regulatory metabolites). This method could also benefit from
351 dynamic data (time-course monitoring in response to metabolic or genetic perturbations). New
352 formalisms will be required to account for *in vivo* conditions, notably the presence of products,
353 similar enzyme and substrate concentrations, local concentration variations, and molecular fluxes
354 within the cell. Our method is particularly valuable for studying membrane-bound and multimeric
355 enzymes, for which the purification and assay optimization steps of classical *in vitro* enzymology can
356 be extremely challenging. For membrane-bound enzymes, *in vivo* enzymology offers a realistic
357 environment devoid of detergents or other interferences, with natural membranes rather than
358 liposomes. We sincerely hope that our work will stimulate further studies delving deeper into how
359 enzymes function in their natural environment.

360

361

362 # Materials and methods

363 ## Plasmid construction

364 Plasmids and primers are listed in Tables EV6-7. Plasmid sequences and annotations are provided in
365 Dataset EV1. The primers were synthesized by IDT (Leuven, Belgium) and the sequences of PaCrtB,
366 PaCrtI and BtCrtI were codon optimized for yeast and synthetized by Twist Bioscience (San Francisco,
367 California). XdCrtE and XdCrtI from *Enterobacter agglomerans* were amplified from pMRI34-CrtE-
368 Gal1-10-HMG1t, YEplac195 YB/I, and pAC-BETA respectively (47–49). Sequences of the mutated
369 versions of the TEF1 promoter TEF1mut2p, TEF1mut5p and TEF1mut7p were obtained from Nevoigt
370 et al. (50). Polymerase chain reaction (PCR) was performed using Phusion high fidelity polymerase
371 and Phire Hot start II DNA polymerase (ThermoFisher Scientific, Lithuania). DNA fragments were
372 purified using Monarch DNA Gel Extraction Kit from New England Biolabs. DNA fragments were
373 annealed by isothermal assembly using NEBuilder HiFi assembly kit from New Englands Biolabs.
374 Clones and plasmids were propagated in homemade calcium- and TOP10-competent *Escherichia coli*
375 cells.

376 ## Construction of yeast strains

377 All yeast strains used in this study are derived from CEN.PK2-1C and are listed in Table EV1. Yeasts
378 were transformed using Gietz et al.'s high-efficiency transformation protocol (51). Integrative
379 cassettes were obtained by enzyme digestion or PCR and were used without any further purification.
380 Strains were selected using auxotrophy markers or antibiotic resistance at a concentration of 400
381 µg/mL. Antibiotic resistance recycling was performed using vector pSH63 as described in the
382 literature (52). Genome integration was verified by colony PCR using the primers listed in Table EV7.
383 Genomic DNA was extracted using DNA release from ThermoFisher Scientific.

384 ## Media and culture conditions

385 All strains were grown in modified synthetic Verduyn media containing glucose (111 mM), NH_4Cl (75
386 mM), KH_2PO_4 (22 mM), $MgSO_4$ (0.4 mM) and CSM (ForMedium LTD, Hunstaton, England) at pH 5.0
387 (53). Sterilization was performed by filtration. Fresh colonies from selective plates were precultured
388 in 350 µL complete synthetic medium at 28 °C for 8 hours and these cells were used to inoculate
389 cultures with a 1:5 medium:flask proportion to an initial OD_{600nm} of 0.002, grown at 200 rpm at 28 °C.

390 ## Carotene quantification

391 Samples (10 or 20 mL) of yeast culture were harvested with an OD_{600nm} of approximately 5,
392 centrifuged, and washed with 1 mL of MilliQ water. Cell pellets were freeze-dried and stored at –80
393 °C until extracted. β-apocarotenal solution (40 µL, 50 µM) was added to the dried cells, and
394 carotenes were extracted with glass beads and 500 µL of acetone in three 20 s rounds of agitation at
395 0.05 m/s with a FastPrep FP120 cell disruptor (ThermoFisher). The acetone phase was transferred to
396 a new tube and the extraction was repeated twice. Acetone extracts were pooled, centrifuged, dried
397 under nitrogen flux, and resuspended in acetone for HPLC analysis. Analyses were carried out on a
398 Thermo Scientific Vanquish Focused UHPLC Plus system with DAD HL. Extract samples (5 µL) were
399 injected into a YMC carotenoid column (100 × 2.0 mm and 3 µm particle size) equipped with a
400 precolumn (100 × 2.0 mm and 3 µm particle size). The mobile phases used to separate and quantify
401 phytoene, lycopene and β-apocarotenal from ergosterol and derivatives were mixtures of (A)
402 methanol/water (95:5) and (B) dichloromethane. The flow was 0.25 mL/min with the following

403 gradient: 0–0.1 min 5 % B, 0.1–0.5 min 20 % B, 0.5–2 min 60 % B, 2–5 min 80 % B, 5–8 min 80 % B
404 and 8–11 min 5 % B. The absorbance from 210 to 600 nm was measured throughout the run with a
405 data collection rate of 2 Hz and a response time of 2 s. The phytoene concentration was deduced
406 from its absorbance at 286 nm and lycopene and β-apocarotenal concentrations from the
407 absorbance at 478 nm. The reference wavelength (600 nm) was subtracted from each of the
408 wavelengths used for metabolite quantification.

409 **Flux calculation**

410 Phytoene and lycopene are produced and accumulate in the cells, and their pools are continuously
411 diluted by cell growth. Assuming an absence of degradation or reutilization of these end-products by
412 the cell, phytoene and lycopene production fluxes are balanced solely by their dilution fluxes in the
413 exponential growth phase, where cells are at metabolic steady-state. Thus, phytoene and lycopene
414 production fluxes were determined by multiplying their concentrations by the cell growth rate. This
415 flux calculation method provides results consistent with those obtained by targeted ^{13}C-fluxomics
416 (54).

417 **GGPP quantification**

418 GGPP was quantified as detailed previously (55). Briefly, 10 mL of broth was filtered through 0.45 µm
419 Sartolon polyamide (Sartorius, Goettingen, Germany) and washed with 5 mL of fresh culture medium
420 (without glucose). The filters were rapidly plunged into liquid nitrogen and then stored at −80 °C until
421 extraction. Intracellular GGPP was extracted by incubating filters in closed glass tubes containing 5
422 mL of an isopropanol/H_20 NH_4HCO_3 100 mM (50/50) mixture at 70 °C for 10 min. For absolute GGPP
423 quantification, 50 µL of ^{13}C internal standard were added to each extract. Cellular extracts were
424 cooled on ice and sonicated for 1 min. Cell debris was removed by centrifugation (5000 g, 4 °C, 5
425 min). Supernatants were evaporated overnight (SC110A SpeedVac Plus, ThermoFisher, Waltham,
426 MA, USA), resuspended in 200 µL of methanol:NH_4OH 10 mM (7:3) at pH 9.5 and stored at −80 °C
427 until analysis.

428 Analyses were carried out on a LC–MS platform composed of a Thermo Scientific Vanquish Focused
429 UHPLC Plus system with DAD HL, coupled to a Thermo Scientific Q Exactive Plus hybrid quadrupole-
430 Orbitrap mass spectrometer (ThermoFisher), as detailed previously (55). Calibration mixtures
431 (prepared at concentrations from 0.08 nM to 10 µM) were used to construct calibration curves from
432 which the absolute concentration of GGPP in the samples was determined.

433 **Western blot**

434 Protein extracts were prepared as described by Zhang et al. (46). Briefly, 1.5 OD_{600nm} of pelleted cells
435 were pre-treated with 100 µL of a 2 M lithium acetate cold solution, and left to stand for 5 min,
436 followed by 5 min centrifugation at 5000 g, 4 °C. The supernatant was discarded and 100 µL of a
437 0.4 M solution of NaOH was added. After gentle resuspension, and 5 min standing on ice, the
438 samples were centrifuged for 5 min at 4 °C. After discarding supernatants, the pellets were
439 vigorously vortexed with 60 µL of bromophenol blue loading dye solution with 5 % β-
440 mercaptoethanol. After denaturation for 10 min at 99 °C, 5 µL of each sample was loaded onto 10
441 % SDS page gel. Semi-dry transfer was performed on PVDF membrane (Merck Millipore, Darmstadt,
442 Germany) using a Trans-Blot SD Cell BioRad apparatus (18 V during 20 min), and 5 % bovine milk in
443 TBS as blocking agent. Incubations were performed with mouse anti-FLAG or mouse anti-V5
444 (ThermoFisher Scientific), and secondary anti-mouse IgG coupled with horseradish peroxidase

445 (ThermoFisher Scientific), diluted according to manufacturer instructions. Proteins were detected by
446 incubation with SuperSignal West Pico PLUS substrate (ThermoFisher Scientific).

447 **Proteomics**

448 For cell disruption, 10^8 cells were dissolved in 200 µL of lysis buffer (0.1 M NaOH, 2 % SDS, 2 % 2-
449 mercaptoethanol, 0.05 M EDTA), heated at 90 °C for 10 min and neutralized with 5 µL of 4 M acetic
450 acid. Glass beads were added and the samples were vortexed at 4 °C for 30 min. Cell debris was
451 pelleted by centrifugation and 3000 g for 10 min and the protein concentration of the supernatant
452 was determined using the Bradford assay. Protein aliquots (400 µg) were cleaned by methanol
453 chloroform precipitation. The protein samples were dissolved in 5 µL of 6 M guanidinium chloride, 5
454 µL of 0.1 M dithiothreitol (DTT), and 100 µL of 50 mM TEAB 50 and diluted to a protein concentration
455 of 2 µg/µL with 90 µL of water. Absolute protein quantification was performed using heavy isotope
456 labeled tryptic peptides as internal standards. Protein lysate aliquots (20 µg) were spiked with a
457 mixture of ten AQUA peptides, C-terminally labeled with heavy lysine or arginine (ThermoFisher
458 Scientific) with concentrations of 50 fmol/µg, 10 fmol/µg, 5 fmol/µg and 0 fmol/µg. The samples
459 were reduced by adding 2 µL of 0.1 M DTT and incubating at 60 °C for 1 h, alkylated with 2 µL of
460 chloroacetamide 0.5 M at room temperature for 30 min, and digested with 0.5 µg of trypsin
461 overnight. Digestion was stopped by adding 5 µL of 1 % TFA and the samples were cleaned using 100
462 µL C18 tips. The extracts were lyophilized, reconstituted in 20 µL of eluent A, and transferred to HPLC
463 vials.

464 Samples were analyzed in triplicate using an UltiMate 3000 UHLC system coupled to a Q Exactive Plus
465 mass spectrometer (ThermoFisher Scientific). Approximately 0.6 µg of peptides were loaded on a C18
466 precolumn (PepMap100, 5 µm, 300 Å, ThermoFisher Scientific) and separated on a PepMap RSLC C18
467 column (50 cm × 75 µm, 2 µm, 100 Å, ThermoFisher Scientific) with a 1.5 h gradient with eluent A
468 (Water, 0.05 % FA) and eluent B (80 % ACN, 0.04 % FA) with a flow rate of 0.3 µL/min. The peptides
469 were first desalted for 4 min at 5 % B, then separated with a gradient to 50 % B over 65 min, to 90 %
470 B in 3 min, held at 90 % B for 8 min, and then equilibrated for 8 min at 4 % B.

471 For targeted absolute quantification, full MS spectra measurements were followed by parallel
472 reaction monitoring (PRM) of targeted heavy AQUA peptides and the corresponding light, native
473 peptide of the proteins of interest. The full MS spectra were acquired in profile mode with the
474 following settings: resolution of 70000, mass range of 350–950 m/z, AGC target of 10^6, and 80 ms
475 maximum injection time. PRM MS2 spectra were acquired with an isolation window of 1.6 m/z,
476 17500 resolution, AGC target of 10^5, 80 ms injection time, and an NCE of 27. The inclusion list
477 contained 26 entries covering the light and heavy species of 10 peptides at the most intense charge
478 state (2+ or 3+).

479 Database searches were performed with Proteome Discoverer (version 3.01.27; ThermoFisher). The
480 raw data were compared with the UniProt protein databases of *S. cerevisiae* strain CEN.PK113-7D
481 (UniProt 02.2023; 5,439 entries), and common contaminants using Sequest HT and Chimerys search
482 algorithms. The Sequest search parameters were a semi-tryptic protease specificity with a maximum
483 of 2 missed cleavage sites. The precursor mass tolerance was 8 ppm and the fragment mass
484 tolerance was 0.02 Da. Oxidation of methionine and acetylation of protein N-termini were allowed as
485 dynamic modifications. Carbamidomethylation of cysteine was set as a static modification. Chimerys
486 database searches were performed with default settings. Percolator q-values were used to restrict

the false discovery rate (FDR) of peptide spectrum matches to 0.01. The FDR of peptide and protein identifications was restricted to 1 % and strict parsimony principles were applied to protein grouping.

A spectral library of the AQUA peptides was generated using Proteome Discoverer with a sample containing only 500 fmol of the ten AQUA peptides, in addition to the PRM analyses of the spiked yeast samples. The PRM data of three concentrations analyzed in triplicate were imported and all transitions were reviewed using Skyline (57). Between four and nine transitions without interference were chosen for each peptide and the ratio of light and heavy peptides of the sum of transitions was calculated for absolute quantification. The list of used peptides and all corresponding transitions are provided in Table EV8.

Calculation of absolute concentrations

Protein and metabolite concentrations are expressed as absolute intracellular concentrations. Metabolite concentrations initially expressed in µmol/g DCW were converted into absolute intracellular concentrations using a conversion factor of 6.59×10^{10} cells/g DCW (Fig EV4) and a cellular volume of 66 μm^3 (58). The intracellular concentrations of PaCrtB and XdCrtI were calculated using a conversion factor of 0.63 g protein/g DCW for yeast grown on ammonium sulfate medium (59). All calculations for data conversion are provided in the corresponding Extended view Tables.

Modeling

To test the impact of enzyme expression level on the obtained kinetic profiles, we built a toy kinetic model of the pathway under study. This model contains two metabolites (GGPP and phytoene) and three reactions: GGPP formation by CrtE, defined as a constant flux; GGPP conversion into phytoene by CrtB, modelled using a Michaelis-Menten rate law; and phytoene dilution by growth, modelled using mass action. The K_M value of CrtB was set arbitrarily to 1, and we simulated the steady-state phytoene production flux and GGPP concentration for three CrtB levels (V_{max} set to 0.02, 0.4 and 0.7) under a broad range of GGPP-producing flux (from 0.01 to 0.4 µM/h). The model has been developed with COPASI v4.39 (60) and is available from our GitHub repository (https://github.com/MetaSys-LISBP/in_vivo_enzymatic_parameters) and from the Biomodels database (61) under accession ID MODEL2407240001. All simulations were performed with COPASI.

Calculation of enzyme parameters

Enzymatic parameters (V_{max} and K_M) were determined by fitting a Michaelis-Menten equation to the measured relationships between substrate concentrations and reaction rates. Uncertainties on fitted parameters were determined using a Monte-Carlo approach. Briefly, 1000 simulated noisy datasets were generated (where the noise was determined as the standard deviation of residuals obtained for the fit of the experimental dataset), and the mean value, standard deviation, and 95 % confidence intervals of each parameter were determined from the distribution of values obtained for the 1000 datasets. For each enzyme, we verified that all parameters were identifiable based on the covariance matrix and on the results of the Monte-Carlo analysis. The code for parameter estimation and statistical analysis is provided as a Jupyter notebook at https://github.com/MetaSys-LISBP/in_vivo_enzymatic_parameters.

Data Availability

The data used to make the figures can be found in the Source Data files. The model and computer code produced in this study are available in the following databases:

- Model: BioModels MODEL2407240001 (https://www.ebi.ac.uk/biomodels/MODEL2407240001)
- Code: GitHub (https://github.com/MetaSys-LISBP/in_vivo_enzymatic_parameters)

Acknowledgements

The authors thank MetaboHub-MetaToul (Metabolomics & Fluxomics facilities, Toulouse, France, https://mth-metatoul.com), which is part of the French National Infrastructure for Metabolomics and Fluxomics (https://www.metabohub.fr), funded by the ANR (MetaboHUB-ANR-11-INBS-0010), for access to MS facilities. The authors also thank Jean-Charles Portais (RESTORE, Geroscience & Rejuvenation Center, Université de Toulouse, INSERM, CNRS, EFS, Toulouse, France), Sylvie Dequin (SPO, Université Montpellier, INRAE, Institut Agro Montpellier, Montpellier, France), Thibault Nidelet (SPO, Université Montpellier, INRAE, Institut Agro Montpellier, Montpellier, France), Thomas Lautier (TBI, Université de Toulouse, CNRS, INRAE, INSA, Toulouse, France) and Sergueï Sokol (TBI, Université de Toulouse, CNRS, INRAE, INSA, Toulouse, France) for insightful discussions.

Competing interests

The authors declare no competing interests.

Funding

This work was supported by the French National Research Agency project ENZINVIVO (ANR-16-CE11-0022).

Contributions

Funding acquisition: CC, SH, PM, GT; Project administration: CC, SH, GT; Conceptualization: CC, SCC, SH, PM, GT; Investigation: SCC, AC, HK, CT, AT, VG, CC, PM; Methodology: SCC, AC, HB, CT, FB, AT, VG, CC, SH, LGA, PM, GT; Software: PM; Formal Analysis: SCC, AC, HB, CT, AT, LGA, PM, GT; Visualization: SCC, PM, GT; Writing – original draft: SCC, PM, GT; Writing – review & editing: SCC, AC, HB, CT, FB, AT, VG, CC, SH, LGA, PM, GT; Supervision: SCC, VG, PM, GT.

References

1. S. R. McGuffee, A. H. Elcock, Diffusion, Crowding & Protein Stability in a Dynamic Molecular Model of the Bacterial Cytoplasm. *PLOS Computational Biology* **6**, e1000694 (2010).
2. B. M. B. Karen van Eunen, The importance and challenges of in vivo-like enzyme kinetics. *Perspectives in Science* **1**, 126–130 (2014).
3. D. Ringe, G. A. Petsko, How Enzymes Work. *Science* **320**, 1428–1429 (2008).
4. A. Sancar, Structure and Function of Photolyase and in Vivo Enzymology: 50th Anniversary. *J. Biol. Chem.* **283**, 32153–32157 (2008).
5. W. Harm, H. Harm, C. S. Rupert, Analysis of photoenzymatic repair of UV lesions in DNA by single light flashes: II. In vivo studies with Escherichia coli cells and bacteriophage. *Mutation Research/Fundamental and Molecular Mechanisms of Mutagenesis* **6**, 371–385 (1968).
6. B. E. Wright, M. H. Butler, K. R. Albe, Systems analysis of the tricarboxylic acid cycle in Dictyostelium discoideum. I. The basis for model construction. *Journal of Biological Chemistry* **267**, 3101–3105 (1992).
7. D. Heckmann, *et al.*, Kinetic profiling of metabolic specialists demonstrates stability and consistency of in vivo enzyme turnover numbers. *Proc Natl Acad Sci USA* 202001562 (2020). https://doi.org/10.1073/pnas.2001562117.
8. D. Davidi, *et al.*, Global characterization of in vivo enzyme catalytic rates and their correspondence to in vitro k_{cat} measurements. *Proc Natl Acad Sci USA* **113**, 3401–3406 (2016).
9. A. Zotter, F. Bäuerle, D. Dey, V. Kiss, G. Schreiber, Quantifying enzyme activity in living cells. *J Biol Chem* **292**, 15838–15848 (2017).
10. S. Bhattacharyya, S. Bershtein, B. V. Adkar, J. Woodard, E. I. Shakhnovich, Metabolic response to point mutations reveals principles of modulation of in vivo enzyme activity and phenotype. *Mol Syst Biol* **17**, e10200 (2021).
11. Y. Takakuwa, H. Nishino, Y. Ishibe, T. Ishibashi, Properties and kinetics of membrane-bound enzymes when both the enzyme and substrate are components of the same microsomal membrane. Studies on lathosterol 5-desaturase. *Journal of Biological Chemistry* **269**, 27889–27893 (1994).
12. M. Camagna, *et al.*, Enzyme Fusion Removes Competition for Geranylgeranyl Diphosphate in Carotenogenesis. *Plant Physiol.* **179**, 1013–1027 (2019).
13. P. Urban, *et al.*, Engineered yeasts simulating P450-dependent metabolisms: tricks, myths and reality. *Drug Metabol Drug Interact* **11**, 169–200 (1994).
14. S. Gemmecker, *et al.*, Phytoene Desaturase from Oryza sativa: Oligomeric Assembly, Membrane Association and Preliminary 3D-Analysis. *PLoS One* **10**, e0131717 (2015).
15. D. Iwata-Reuyl, S. K. Math, S. B. Desai, C. D. Poulter, Bacterial Phytoene Synthase:? Molecular Cloning, Expression, and Characterization of Erwinia herbicola Phytoene Synthase†. *Biochemistry* **42**, 3359–3365 (2003).
16. P. Schaub, *et al.*, On the Structure and Function of the Phytoene Desaturase CRTI from Pantoea ananatis, a Membrane-Peripheral and FAD-Dependent Oxidase/Isomerase. *PLoS ONE* **7**, e39550 (2012).
17. M. Fournié, G. Truan, Multiplicity of carotene patterns derives from competition between phytoene desaturase diversification and biological environments. *Sci Rep* **10**, 21106 (2020).
18. P. Stickforth, G. Sandmann, Structural and kinetics properties of a mutated phytoene desaturase from Rubrivivax gelatinosus with modified product specificity. *Arch Biochem Biophys* **505**, 118–122 (2011).
19. L. Michaelis, M. Menten, Die Kinetik der Invertinwirkung. *Biochemische Zeitschrift* **49**, 333–369 (1913).
20. F. J. Bruggeman, J. J. Hornberg, F. C. Boogerd, H. V. Westerhoff, Introduction to systems biology. *EXS* **97**, 1–19 (2007).

21. U. Neudert, I. M. Martínez-Férez, P. D. Fraser, G. Sandmann, Expression of an active phytoene synthase from Erwinia uredovora and biochemical properties of the enzyme. *Biochimica et Biophysica Acta (BBA) - Lipids and Lipid Metabolism* **1392**, 51–58 (1998).
22. P. D. Fraser, W. Schuch, P. M. Bramley, Phytoene synthase from tomato (Lycopersicon esculentum) chloroplasts – partial purification and biochemical properties. *Planta* **211**, 361–369 (2000).
23. B. Camara, "[32] Plant phytoene synthase complex: Component enzymes, immunology, and biogenesis" in *Methods in Enzymology*, Carotenoids Part B: Metabolism, Genetics, and Biosynthesis., (Academic Press, 1993), pp. 352–365.
24. A. Schofield, G. Paliyath, Modulation of carotenoid biosynthesis during tomato fruit ripening through phytochrome regulation of phytoene synthase activity. *Plant Physiology and Biochemistry* **43**, 1052–1060 (2005).
25. G. Sandmann, Evolution of carotene desaturation: The complication of a simple pathway. *Archives of Biochemistry and Biophysics* **483**, 169–174 (2009).
26. J. Koschmieder, *et al.*, Plant-type phytoene desaturase: Functional evaluation of structural implications. *PLoS ONE* **12**, e0187628 (2017).
27. H. Rabeharindranto, *et al.*, Enzyme-fusion strategies for redirecting and improving carotenoid synthesis in *S. cerevisiae*. *Metab Eng Commun* **8**, e00086 (2019).
28. Y. Chen, *et al.*, Lycopene overproduction in *Saccharomyces cerevisiae* through combining pathway engineering with host engineering. *Microbial Cell Factories* **15**, 113 (2016).
29. P. J. Westfall, *et al.*, Production of amorphadiene in yeast, and its conversion to dihydroartemisinic acid, precursor to the antimalarial agent artemisinin. *PNAS* **109**, E111–E118 (2012).
30. J. Zhao, *et al.*, Dynamic control of ERG20 expression combined with minimized endogenous downstream metabolism contributes to the improvement of geraniol production in *Saccharomyces cerevisiae*. *Microb Cell Fact* **16**, 1–11 (2017).
31. A. Faulkner, *et al.*, The LPP1 and DPP1 Gene Products Account for Most of the Isoprenoid Phosphate Phosphatase Activities inSaccharomyces cerevisiae. *J. Biol. Chem.* **274**, 14831–14837 (1999).
32. B. Peng, L. K. Nielsen, S. C. Kampranis, C. E. Vickers, Engineered protein degradation of farnesyl pyrophosphate synthase is an effective regulatory mechanism to increase monoterpene production in Saccharomyces cerevisiae. *Metabolic Engineering* **47**, 83–93 (2018).
33. C. Chambon, V. Ladeveze, A. Oulmouden, M. Servouse, F. Karst, Isolation and properties of yeast mutants affected in farnesyl diphosphate synthetase. *Curr Genet* **18**, 41–46 (1990).
34. K. Tokuhiro, *et al.*, Overproduction of Geranylgeraniol by Metabolically Engineered Saccharomyces cerevisiae. *Appl. Environ. Microbiol.* **75**, 5536–5543 (2009).
35. X. Zhou, *et al.*, Phytoene Synthase: The Key Rate-Limiting Enzyme of Carotenoid Biosynthesis in Plants. *Frontiers in Plant Science* **13** (2022).
36. D. Leys, J. Basran, F. Talfournier, M. J. Sutcliffe, N. S. Scrutton, Extensive conformational sampling in a ternary electron transfer complex. *Nat Struct Mol Biol* **10**, 219–225 (2003).
37. L. Phégnon, *et al.*, Phosphogluconolactonase as the linchpin of an efficient pentose phosphate pathway. [Preprint] (2023). Available at: https://www.biorxiv.org/content/10.1101/2023.11.29.569206v2 [Accessed 8 December 2023].
38. J. O. Park, *et al.*, Metabolite concentrations, fluxes and free energies imply efficient enzyme usage. *Nat Chem Biol* **12**, 482–489 (2016).
39. X. Bu, J. Lin, C. Duan, M. A. G. Koffas, G. Yan, Dual regulation of lipid droplet-triacylglycerol metabolism and ERG9 expression for improved β-carotene production in Saccharomyces cerevisiae. *Microb Cell Fact* **21**, 3 (2022).
40. Y. Zhu, *et al.*, Enhanced synthesis of Coenzyme Q10 by reducing the competitive production of carotenoids in Rhodobacter sphaeroides. *Biochemical Engineering Journal* **125**, 50–55 (2017).
41. R. Heinrich, T. A. Rapoport, A linear steady-state treatment of enzymatic chains. General properties, control and effector strength. *Eur J Biochem* **42**, 89–95 (1974).

657 42. H. Kacser, J. A. Burns, The control of flux. *Symp Soc Exp Biol* **27**, 65–104 (1973).
658 43. B. Enjalbert, P. Millard, M. Dinclaux, J.-C. Portais, F. Létisse, Acetate fluxes in Escherichia coli are
659 determined by the thermodynamic control of the Pta-AckA pathway. *Sci Rep* **7**, 42135 (2017).
660 44. S.-M. Fendt, *et al.*, Tradeoff between enzyme and metabolite efficiency maintains metabolic
661 homeostasis upon perturbations in enzyme capacity. *Mol Syst Biol* **6**, 356 (2010).
662 45. P. Millard, K. Smallbone, P. Mendes, Metabolic regulation is sufficient for global and robust
663 coordination of glucose uptake, catabolism, energy production and growth in Escherichia coli.
664 *PLOS Computational Biology* **13**, e1005396 (2017).
665 46. M. L. Reaves, B. D. Young, A. M. Hosios, Y.-F. Xu, J. D. Rabinowitz, Pyrimidine homeostasis is
666 accomplished by directed overflow metabolism. *Nature* **500**, 237–241 (2013).
667 47. R. Verwaal, *et al.*, High-Level Production of Beta-Carotene in Saccharomyces cerevisiae by
668 Successive Transformation with Carotenogenic Genes from Xanthophyllomyces dendrorhous.
669 *Appl. Environ. Microbiol.* **73**, 4342–4350 (2007).
670 48. F. X. Cunningham Jr, *et al.*, Functional analysis of the beta and epsilon lycopene cyclase
671 enzymes of Arabidopsis reveals a mechanism for control of cyclic carotenoid formation. *The*
672 *Plant Cell* **8**, 1613–1626 (1996).
673 49. W. Xie, *et al.*, Construction of a controllable β-carotene biosynthetic pathway by decentralized
674 assembly strategy in Saccharomyces cerevisiae. *Biotechnol. Bioeng.* **111**, 125–133 (2014).
675 50. Engineering of Promoter Replacement Cassettes for Fine-Tuning of Gene Expression in
676 Saccharomyces cerevisiae | Applied and Environmental Microbiology. Available at:
677 https://journals-asm-org.insb.bib.cnrs.fr/doi/10.1128/aem.00530-06 [Accessed 30 January
678 2024].
679 51. R. D. Gietz, Yeast transformation by the LiAc/SS carrier DNA/PEG method. *Methods Mol. Biol.*
680 **1205**, 1–12 (2014).
681 52. U. Güldener, S. Heck, T. Fiedler, J. Beinhauer, J. H. Hegemann, A New Efficient Gene Disruption
682 Cassette for Repeated Use in Budding Yeast. *Nucl. Acids Res.* **24**, 2519–2524 (1996).
683 53. C. Verduyn, E. Postma, W. A. Scheffers, J. P. Y. 1990 van Dijken, Physiology of Saccharomyces
684 Cerevisiae in Anaerobic Glucose-Limited Chemostat Culturesx. *Microbiology* **136**, 395–403.
685 54. P. Millard, *et al.*, ScalaFlux: A scalable approach to quantify fluxes in metabolic subnetworks.
686 *PLOS Computational Biology* **16**, e1007799 (2020).
687 55. S. Castaño-Cerezo, *et al.*, Functional analysis of isoprenoid precursors biosynthesis by
688 quantitative metabolomics and isotopologue profiling. *Metabolomics* **15**, 115 (2019).
689 56. T. Zhang, *et al.*, An improved method for whole protein extraction from yeast Saccharomyces
690 cerevisiae. *Yeast* **28**, 795–798 (2011).
691 57. B. MacLean, *et al.*, Effect of Collision Energy Optimization on the Measurement of Peptides by
692 Selected Reaction Monitoring (SRM) Mass Spectrometry. *Anal. Chem.* **82**, 10116–10124 (2010).
693 58. N. Punekar, "In Vitro Versus In Vivo: Concepts and Consequences" in *ENZYMES: Catalysis,*
694 *Kinetics and Mechanisms*, Springer Singapore, (2018), pp. 493–519.
695 59. E. Albers, C. Larsson, G. Lidén, C. Niklasson, L. Gustafsson, Influence of the nitrogen source on
696 *Saccharomyces cerevisiae* anaerobic growth and product formation. *Appl Environ Microbiol* **62**,
697 3187–3195 (1996).
698 60. COPASI—a COmplex PAthway SImulator | Bioinformatics | Oxford Academic. Available at:
699 https://academic.oup.com/bioinformatics/article/22/24/3067/208398 [Accessed 25 July 2024].
700 61. R. S. Malik-Sheriff, *et al.*, BioModels—15 years of sharing computational models in life science.
701 *Nucleic Acids Research* **48**, D407–D415 (2020).

702

703

704 **Figure legends**

705 **Figure 1. General principle of the proposed strategy for *in vivo* enzymology and comparison**
706 **between *in vitro* and *in vivo* enzymology approaches.**

707 **Figure 2**. **Scheme of the construction of yeast strains with different GGPP concentration.** Red filled
708 dots represent a copy of GGPP synthase, and empty dots represent an empty integration cassette.

709 **Figure 3. Construction of the set of yeast strains with different intracellular GGPP concentrations.**

710 A Genomic modification scheme for the yENZ15 strain and intracellular fates of GGPP in *S. cerevisiae.*
711 Overexpressed enzymes are shown in blue, enzyme deletion is shown in red, and enzyme modulation
712 is shown in green.

713 B GGPP concentration (green bars) and specific growth rate of *S. cerevisiae* strains (orange dots).
714 Mean values ± standard deviations (error bars) were estimated from three independent biological
715 replicates.

716 **Figure 4. *In vivo* characterization of phytoene synthase from *Pantoea ananas*.**

717 A Scheme for the biosynthesis of phytoene by CrtB.

718 B Steady-state flux and substrate concentration simulated for three different CrtB activities (low,
719 medium and high) under a broad range of GGPP-producing flux.

720 C *In vivo* characterization of CrtB in *S. cerevisiae*: phytoene production as a function of GGPP
721 concentration in strains with low (TEF1mut2p), medium (PGIp) and high (PDC1p) level of CrtB. Each
722 data point represents an independent biological replicate. For PGIp strains, red line represents the
723 best fit of a Michaelis-Menten rate law, and shaded area corresponds to 95 % confidence interval on
724 the fit.

725 **Figure 5. *In vivo* characterization of three phytoene desaturases.**

726 A Scheme for the biosynthesis of lycopene by CrtI.

727 B–D *In vivo* characterization of CrtI from *P. ananas* (B), *X. dendrorus* (C) and *B. trispora* (D). Each data
728 point represents an independent biological replicate, red lines represent the best fits of a Michaelis-
729 Menten rate law, and shaded areas correspond to 95 % confidence intervals on the fits.

730

731 **Expanded View Figure legends**

732 **Figure EV1.** PaCrtB-FLAG expression determined by western blot in yeast strains with different GGPP
733 concentrations (panels A, B and C correspond to three different biological replicates).

734 **Figure EV2.** Lycopene production in *S. cerevisiae*.

735 A *S. cerevisiae* yGGPP34 strain expressing PDC1p-PaCrtB and TDH3p-BtCrtI. Bright field images were
736 acquired using the camera LEICA DFC300FX mounted in the microscope Leica DM4000B with Leica
737 EL6000 light source. Lycopene crystals are observed in red.

738 B Decrease of specific growth rate in yeast strains expressing BtCrtI with different phytoene
739 concentrations.

740 **Figure EV3**. Expression of the three studied CrtI-V5 proteins in strains with low (yGGPP030) and high
741 (yGGPP044) phytoene content (panels A and B correspond to three different biological replicates).

742 **Figure EV4**. Correlation between cell/mL and OD_{600nm} (A) and between OD_{600nm} and mg DCW (B).

743

744 **Expanded View Table legends Table EV1.** Yeast strains used in this study.

745 **Table EV2.** PaCrtB and XdCrtI absolute protein quantification.

746 **Table EV3.** Enzymatic parameters measured *in vivo*.

747 **Table EV4.** *In vitro* parameters of bacterial phytoene synthase and phytoene desaturase.

748 **Table EV5.** Molecule number of each component for the *in vivo* enzymology reaction.

749 **Table EV6.** Plasmids used in this study.

750 **Table EV7.** Primers used for colony PCRs.

751 **Table EV8.** Peptides and PRM transitions used for absolute quantification of the enzymes.

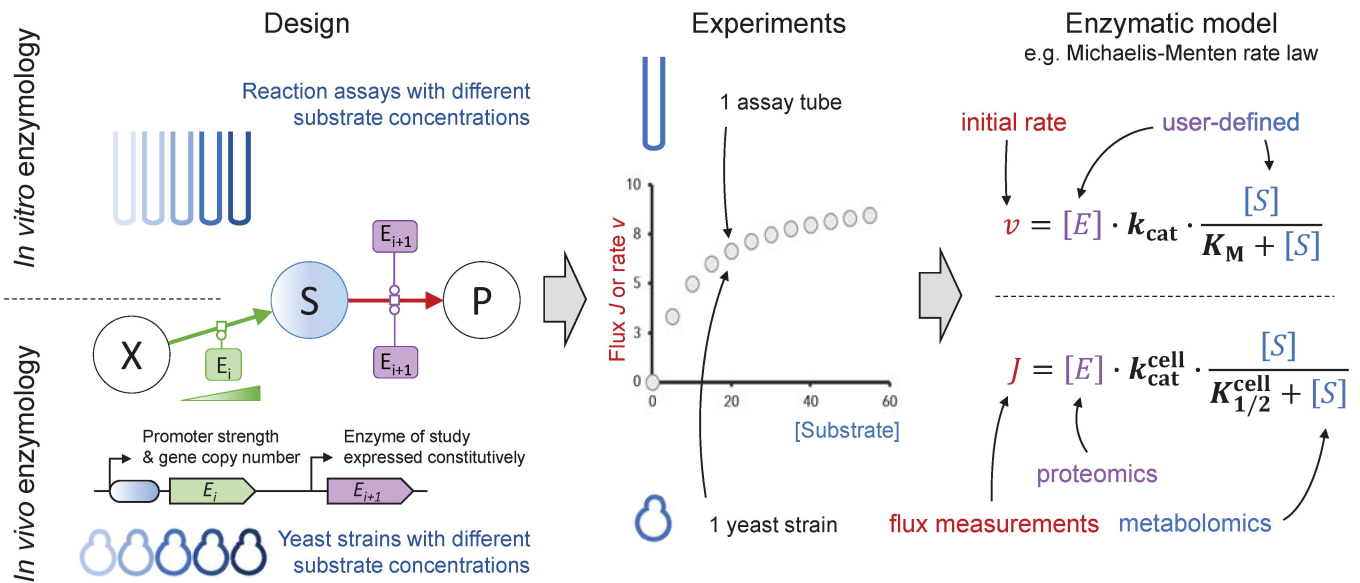
Design
Experiments
Enzymatic model
e.g. Michaelis-Menten rate law
In vitro enzymology
Reaction assays with different substrate concentrations
X
S
P
E_i
E_{i+1}
E_{i+1}
1 assay tube
Flux J or rate v
[Substrate]
initial rate
user-defined
$v = [E] \cdot k_{cat} \cdot \frac{[S]}{K_M + [S]}$
In vivo enzymology
Promoter strength & gene copy number
Enzyme of study expressed constitutively
E_i
E_{i+1}
Yeast strains with different substrate concentrations
1 yeast strain
$J = [E] \cdot k_{cat}^{cell} \cdot \frac{[S]}{K_{1/2}^{cell} + [S]}$
proteomics
flux measurements
metabolomics

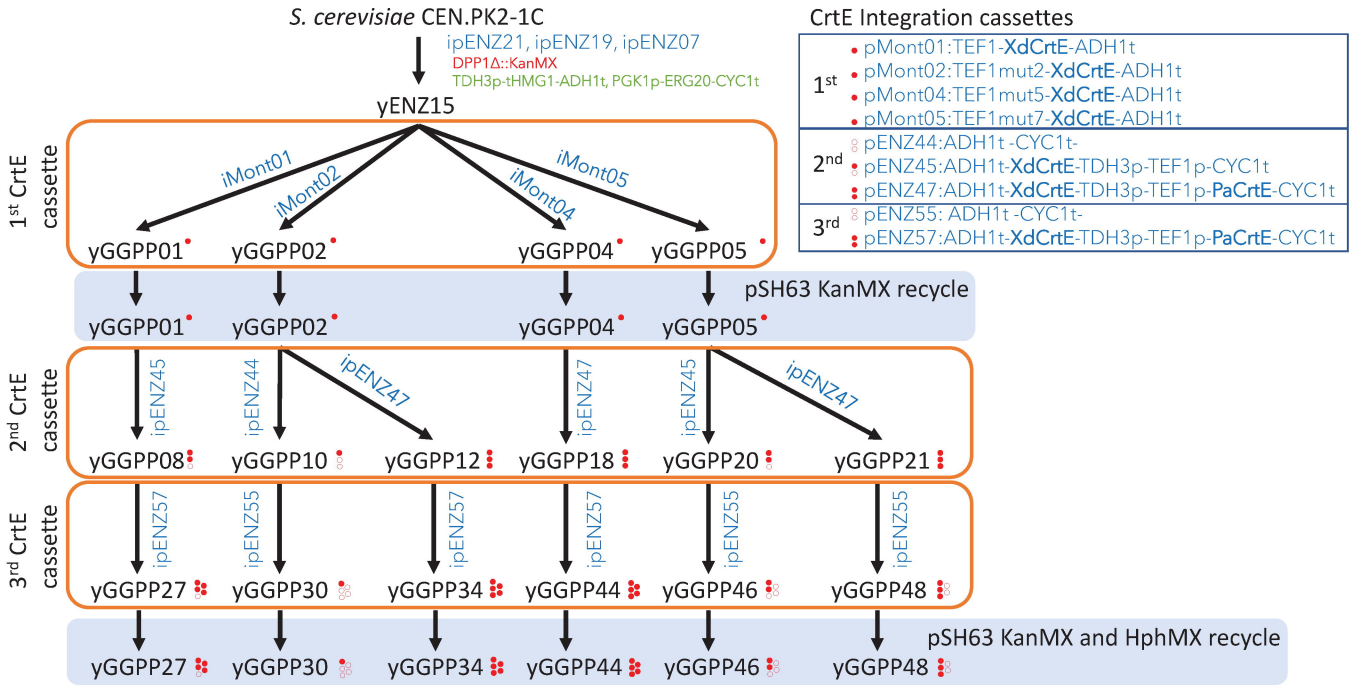
S. cerevisiae CEN.PK2-1C
ipENZ21, ipENZ19, ipENZ07
DPP1Δ::KanMX
TDH3p-tHMG1-ADH1t, PGK1p-ERG20-CYC1t
yENZ15
1st CrtE cassette
iMont01
iMont02
iMont04
iMont05
yGGPP01
yGGPP02
yGGPP04
yGGPP05
pSH63 KanMX recycle
yGGPP01
yGGPP02
yGGPP04
yGGPP05
2nd CrtE cassette
ipENZ45
ipENZ44
ipENZ47
ipENZ47
ipENZ45
ipENZ47
yGGPP08
yGGPP10
yGGPP12
yGGPP18
yGGPP20
yGGPP21
3rd CrtE cassette
ipENZ57
ipENZ55
ipENZ57
ipENZ57
ipENZ55
ipENZ55
yGGPP27
yGGPP30
yGGPP34
yGGPP44
yGGPP46
yGGPP48
pSH63 KanMX and HphMX recycle
yGGPP27
yGGPP30
yGGPP34
yGGPP44
yGGPP46
yGGPP48
CrtE Integration cassettes
1st
pMont01:TEF1-XdCrtE-ADH1t
pMont02:TEF1mut2-XdCrtE-ADH1t
pMont04:TEF1mut5-XdCrtE-ADH1t
pMont05:TEF1mut7-XdCrtE-ADH1t
2nd
pENZ44:ADH1t -CYC1t-
pENZ45:ADH1t-XdCrtE-TDH3p-TEF1p-CYC1t
pENZ47:ADH1t-XdCrtE-TDH3p-TEF1p-PaCrtE-CYC1t
3rd
pENZ55: ADH1t -CYC1t-
pENZ57:ADH1t-XdCrtE-TDH3p-TEF1p-PaCrtE-CYC1t

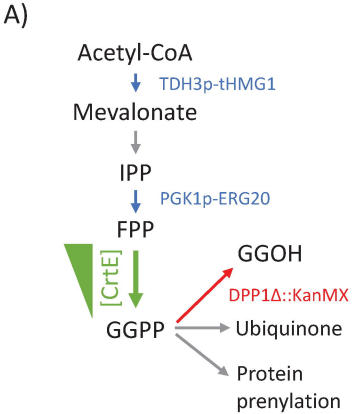
A)
Acetyl-CoA
TDH3p-tHMG1
Mevalonate
IPP
PGK1p-ERG20
FPP
[CrtE]
GGOH
DPP1Δ::KanMX
GGPP
Ubiquinone
Protein
prenylation

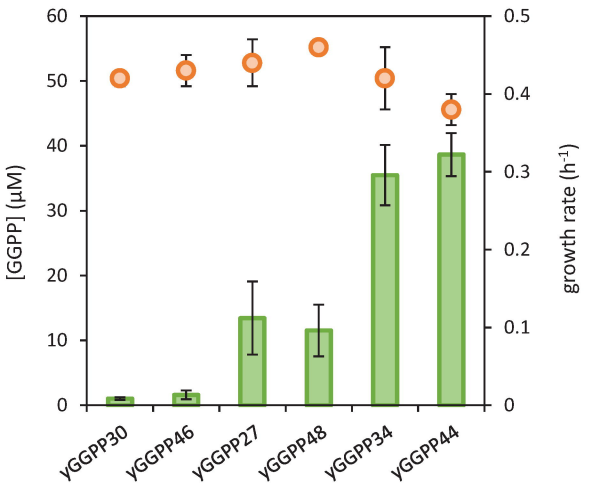
B)
[GGPP] (μM)
growth rate (h-1)
0
10
20
30
40
50
60
0
0.1
0.2
0.3
0.4
0.5
yGGPP30
yGGPP46
yGGPP27
yGGPP48
yGGPP34
yGGPP44

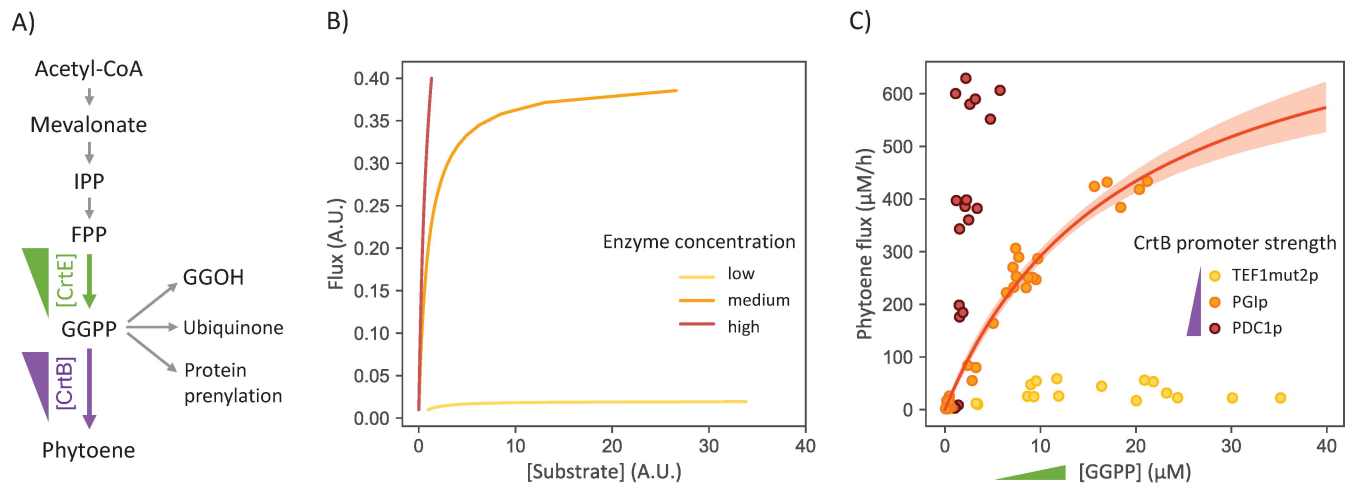
A)
Acetyl-CoA
Mevalonate
IPP
FPP
[CrtE]
GGPP
GGOH
Ubiquinone
Protein prenylation
[CrtB]
Phytoene
B)
Flux (A.U.)
[Substrate] (A.U.)
Enzyme concentration
low
medium
high
C)
Phytoene flux (µM/h)
[GGPP] (µM)
CrtB promoter strength
TEF1mut2p
PGIp
PDC1p

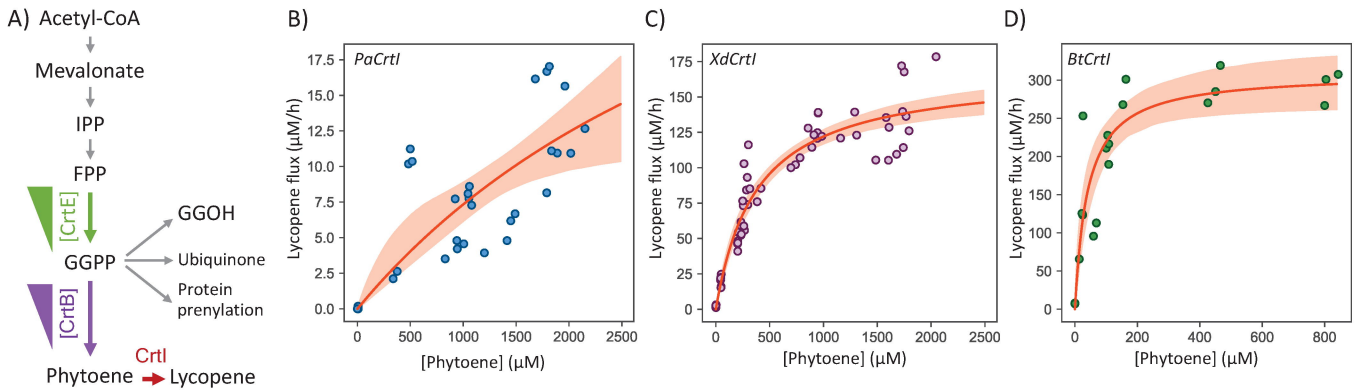
A)
Acetyl-CoA
Mevalonate
IPP
FPP
[CrtE]
GGPP
GGOH
Ubiquinone
Protein prenylation
[CrtB]
CrtI
Phytoene
Lycopene
B)
PaCrtI
Lycopene flux (μM/h)
[Phytoene] (μM)
C)
XdCrtI
Lycopene flux (μM/h)
[Phytoene] (μM)
D)
BtCrtI
Lycopene flux (μM/h)
[Phytoene] (μM)